Power exchange dynamics for performance optimization in a miniature plasmonic waveguide coupler

MANOJ MISHRA[a], PUJA JHAJHARIA[a], SOUMENDU JANA[b,*]
[a]*Department of Physics, SLAS, Mody University of Science and Technology, Lakshmangarh-332311, Sikar, Raj, India*
[b]*School of Physics and Materials Science, Thapar Institute of Engineering and Technology, Patiala, Punjab-147004, India*

This article considers a miniature MIMIM waveguide plasmonic coupler and presents the power exchange dynamics in it. The role of the system parameters as well as the operating wavelength on the coupling dynamics is identified. The field dynamics has been simulated using finite-difference time-domain (FDTD) based numerical method. The investigation will help to design an experimental miniature plasmonic waveguide coupler and to optimize the same.

(Received October 6, 2020; accepted June 11, 2021)

Keywords: Surface Plasmon Polariton, Directional coupler, FDTD method

1. Introduction

The miniaturization of photonic devices has been one of the main thrust areas of research in many industries and so in the optoelectronics industry [1]. A large variety of 'on-chip' versions of many optoelectronic devices are emerging without any compromise with the performance [2]. Moreover, the photonic devices are struggling to match the scale of miniaturization already attained by their electronic counterparts. The progress of photonic crystal technology endows with the size reduction of optical components (e.g., waveguides and couplers) by at least one order of magnitude in comparison to their conventional version that relies on the total internal reflection. The *diffraction limit* is the main challenge in achieving further miniaturization up-to nano-scale. However, *plasmonics*, aided by surface plasmon, surface plasmon resonance and surface plasmon polaritons (SPP) showed a new path to break this limit [3]. *Plasmons* are basically quasi-particles resulting from the quantization of plasma or the free electron (or ion) gas. Plasmon can be created within the bulk or on the surface. The plasmon created along the metal and dielectric interface is b recognized as *surface plasmon* (SP). See the work of Rufus Ritchie [4] who first predicted SP in 1957. SP possess lower (theoretically, $\sqrt{2}$ times lower) energy than that of the bulk (or volume) plasmons. Interaction of SP with the optical photon may result in a hybrid excitation, namely *surface plasmon polaritons* (SPP). SPP can be viewed as an evanescent wave trapped at the interface between two media, one having positive dielectric constant, while the other has negative one. For example, the interface of air and noble metals is a suitable system for hosting SPP. Generally, SPP propagates along the interface until complete dissipation of its energy through radiative loss or absorption in the metal. However the loss can be compensated by a gain from the neighbouring dielectric [5]. With time, SPP and, in fact, *plasmonics* [6] have found a significantly large number and variety of applications from biological nano-sensors [7], to sub-wavelength imaging [8] and from the merging of electronic circuits to photonic devices [9]. Furthermore, SPP plays the key role in numerous nano-scale optical passive devices like Bragg reflectors [10], bends and splitters [11], directional couplers [12-19], long-range nanoware waveguide [20], passive filters [21], and Mach-Zehnder interferometers [22]. SPP has been used in Raman spectroscopy [23], high-resolution optical microscopy [24], magneto-optic effect [25], optical amplification and quantum information processing. Even polymer based SPP waveguides are developed for high speed optical communication [26]. Please see [27] for SPP amplifiers and lasers, ref [28] for nano-optics of SPP and ref [29] for the physics and applications of SPP.

This article presents the power exchange dynamics of a miniature plasmonic coupler having metal-insulator-metal-insulator-metal (MIMIM) structure. The multilayer metallic waveguides are interesting plasmonic structures as they produce waveguide couplers, beam splitters and integrated modulators in optoelectronic devices. Although the MIMIM structure or MIM coupler is familiar and well reported, the current investigation provides the basic but important transmission dynamics for a large operating range and hence can be directly adopted for the experimental setup. Moreover, following our main agenda we consider a miniature plasmonic waveguide coupler.

Fig. 1. Schematic of the MIMIM Plasmonic waveguide coupler

2. The model

We consider a five-layer metal-insulator-metal-insulator-metal (MIMIM) structure as shown in Fig. 1. The thickness is so small with respect to the span of the structure that it can be considered as a two dimensional (2D) structure. The structure is formed by making two parallel grooves on a metal (Silver) sheet. Since the two grooves are filled with air (dielectric) the whole structure is now equivalent to a pair of coupled MIM waveguides that can behave like a 2 × 2 directional plasmonic coupler. These two air grooves each of length 'L' and width 'a' are '$2d$' distance apart from each other. In such a system every single interface contains bound SPPs. In principle, the SP can be created by the interaction of photons with metallic nano structure. Basically, two configurations are popular for the generation of SP; the Otto configuration [1] and the Kretschmann configuration (or Kretschmann–Raether configuration) [1]. In the present case the fundamental TM mode of the plasmonic waveguide is excited by a dipole source [31]. When the separation between adjacent interfaces is smaller than the decay length (along $\hat{z}$) of the interface modes an interaction takes place between the said modes. Such interaction in the coupled-waveguide-directional-coupler can be analytically modeled by coupled-mode theory for uniform couplers [30]. The dynamics of the field amplitudes of the plasmonic waveguides can be presented by the following coupled-mode equations:

$$\frac{\partial a_1}{\partial z} = -j\delta a_1 - j\kappa a_2, \tag{1}$$

$$\frac{\partial a_2}{\partial z} = -j\delta a_2 - j\kappa a_1 \tag{2}$$

where a_1 and a_2 are the field in the waveguide-1 and waveguide-2 respectively. κ is the coupling coefficient and δ is the phase-mismatch factor.

The dispersion relation of the plasmonic coupler can be determined as follows. It is well known that a plasmonic waveguide supports only TM mode [1]. For the present case the TM field components can be determined as:

$$H_y = \begin{cases} Ae^{i\beta x}e^{-k_m z} & (I) \\ Be^{i\beta x}e^{-k_i z} + Ce^{i\beta x}e^{k_i z} & (II) \\ De^{i\beta x}e^{-k_m z} + Ee^{i\beta x}e^{k_m z} & (III) \\ Fe^{i\beta x}e^{-k_i z} + Ge^{i\beta x}e^{k_i z} & (IV) \\ He^{i\beta x}e^{k_m z} & (V) \end{cases} \tag{3}$$

and

$$E_x = \begin{cases} iA\dfrac{1}{\omega\varepsilon_0\varepsilon_m}k_m e^{i\beta x}e^{-k_m z} & (I) \\ iB\dfrac{1}{\omega\varepsilon_0\varepsilon_i}k_i e^{i\beta x}e^{-k_i z} - iC\dfrac{1}{\omega\varepsilon_0\varepsilon_i}k_i e^{i\beta x}e^{k_i z} & (II) \\ iD\dfrac{1}{\omega\varepsilon_0\varepsilon_m}k_m e^{i\beta x}e^{-k_m z} - iE\dfrac{1}{\omega\varepsilon_0\varepsilon_m}k_m e^{i\beta x}e^{k_m z} & (III) \\ iF\dfrac{1}{\omega\varepsilon_0\varepsilon_i}k_i e^{i\beta x}e^{-k_i z} - iG\dfrac{1}{\omega\varepsilon_0\varepsilon_i}k_i e^{i\beta x}e^{k_i z} & (IV) \\ -iH\dfrac{1}{\omega\varepsilon_0\varepsilon_m}k_m e^{i\beta x}e^{k_m z} & (V) \end{cases} \tag{4}$$

where $k_m = \left(\beta^2 - k_0^2\varepsilon\right)^{1/2}$, $k_i = \left(\beta^2 - k_0^2\varepsilon\right)^{1/2}$. β presents the longitudinal wave number. *A, B, C, D, E, F, G* and *H* represent the field amplitudes at the interfaces, namely, $z = a + d$, $z = d$, $z = -d$, $z = -a - d$ respectively. In the above expressions of H_y and E_x the (I)-(V) represent the ranges of z corresponding to the expressions in its left. The range is as follows: *(I)* $(a + d) < z$, *(II)* $(a + d) < z < d$, *(III)* $d < z < -d$, *(IV)* $-d < z < (-a - d)$ and *(V)* $z < (-a - d)$. According to the boundary conditions the longitudinal tangential component of the electric field E_x and and transverse normal component of the magnetic field H_y are continuous across the interfaces. The normal component of the electric field and the parallel component of the magnetic field are discontinuous. This leads to the dispersion relations as follows:

$$\begin{aligned} &(R-S)^2(R+S)^2 e^{k_m(-2a-4d)-2k_i a} \\ &+(R-S)^2(R+S)^2 e^{k_m(-2a-4d)+2k_i a} \\ &-(R+S)^4 e^{2a(k_i-k_m)} - (R-S)^2 \\ &\left(2(R+S)^2 e^{-2k_m(a+2d)} + (R-S)^2 e^{-2a(k_i+k_m)}\right. \\ &-2e^{-2k_m a}(R+S)^2 = 0 \end{aligned} \tag{5}$$

where $R = k_m/\varepsilon_m$ and $S = k_i/\varepsilon_i$

3. Simulation results and analysis

The transmission characteristics and power exchange dynamics of the aforesaid plasmonic coupler is investigated by direct numerical simulation using the finite-difference time-domain (FDTD) method. An electromagnetic (EM) radiation is injected through the waveguide-1 along the positive x-axis and the output power is recorded at both waveguides. The transmission spectra as well as field dynamics through the waveguides are investigated by varying the separation between waveguides ('d') and the length of waveguides ('L'). A wide variety of electromagnetic radiation of wavelength ('λ') ranging from 600 nm to 1600 nm is used for revealing the field dynamics in the coupler as portrayed hereafter.

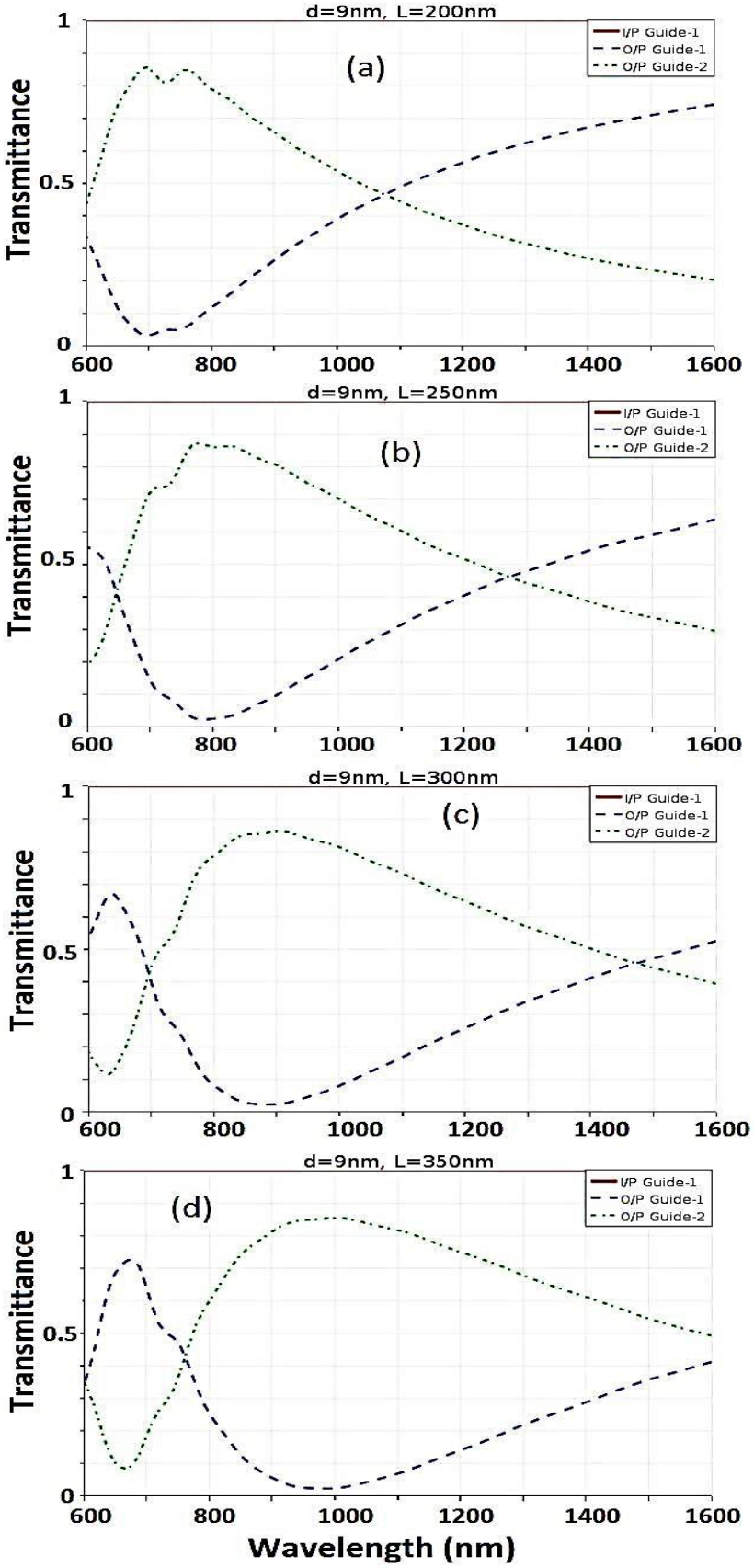

Fig. 2. Transmittance spectra of waveguide-1 and waveguide-2 for d = 9 nm and for waveguide lengths (a) L = 200 nm (b) L = 250 nm (c) L = 300 nm and (d) L = 350 nm. Solid line is for input power, dashed and dotted lines are for powers in waveguide-1 and waveguide-2 respectively (color online)

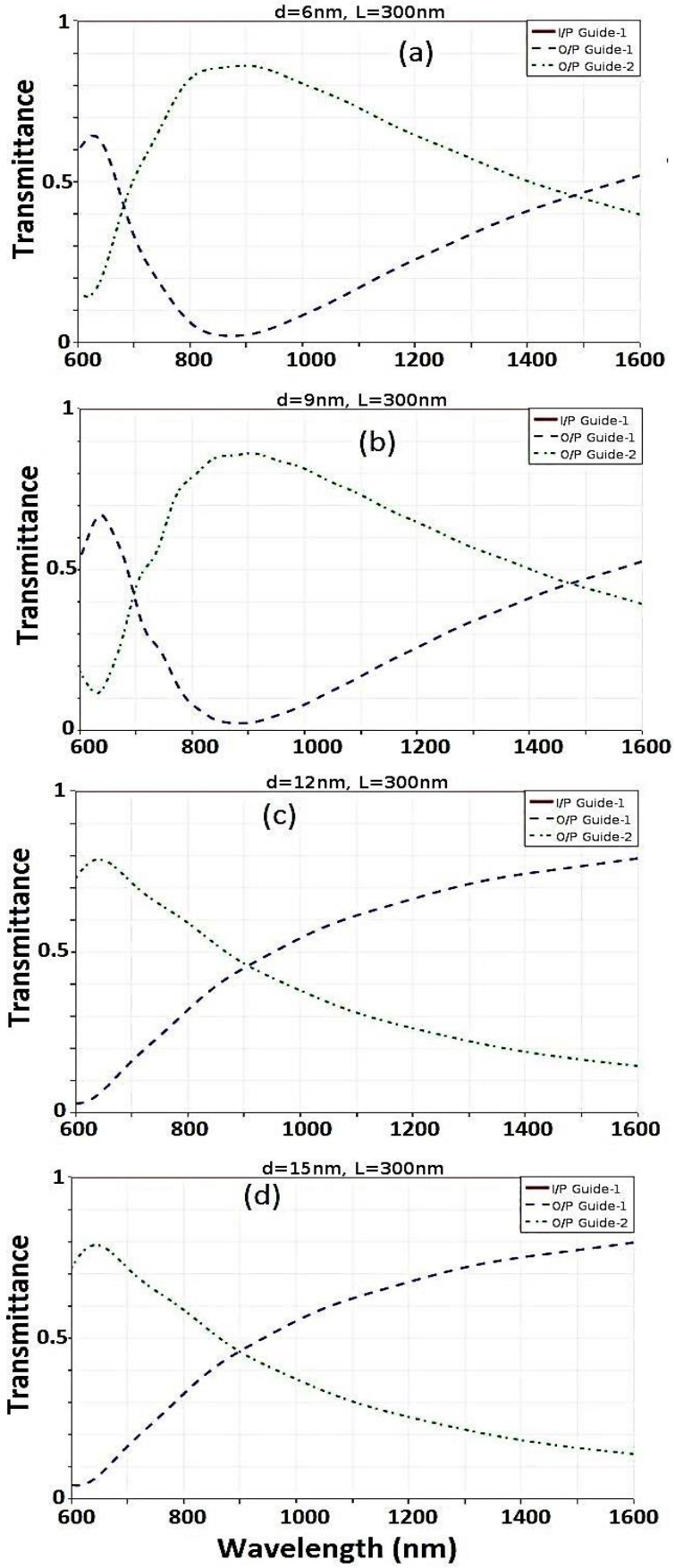

Fig. 3. Transmittance spectra of waveguide-1 and waveguide-2 for L = 300 nm and for (a) d = 6 nm, (b) d = 9 nm, (c) d = 12 nm and (d) d = 15 nm. The solid line is for input power, dashed and dotted lines are for powers in waveguide-1 and waveguide-2 espectively (color online)

Firstly, we explore the role of the length of the waveguide on the transmittance spectra of the coupler. As a common norm, the EM radiation is injected in the waveguide-1 and the power transmission is recorded at the output end of both the waveguides. Fig. 2 presents the power transmission for varying wavelengths of the input EM radiation. The separation between dielectric waveguides is maintained at d = 9 nm and the value of parameter '*a*' (i.e., width of air grooves) is 50 nm. This particular value of '*a*' is taken so that only the fundamental transverse magnetic (TM0) mode can be supported by the structure. [31]. Increase in the value of '*a*' may lead to generation of multiple modes and hence operational complexities. The transmittance, i.e., ratio of amplitudes of the output end to that at the input end, is recorded for coupler lengths L = 200 nm, 250 nm, 300 nm, and 350 nm respectively. It is clear from the figure that the powers in the waveguides are different at different values of '*L*' and are highly dependent on the wavelength (or frequency) of the EM radiation. There is a (or two) wavelength(s) at which the powers in both the waveguides are the same, i.e., at this (these) wavelength(s) the coupler behaves like a beam splitter. Such beam-splitting point shifts towards the higher wavelength side (red-shifted) with increase in the coupler length. These plots also show the maximum power coupling frequencies for a given coupler. The simulation can help to choose a desired role of the coupler for a given wavelength and coupler length. In fact one can make a chart of it.

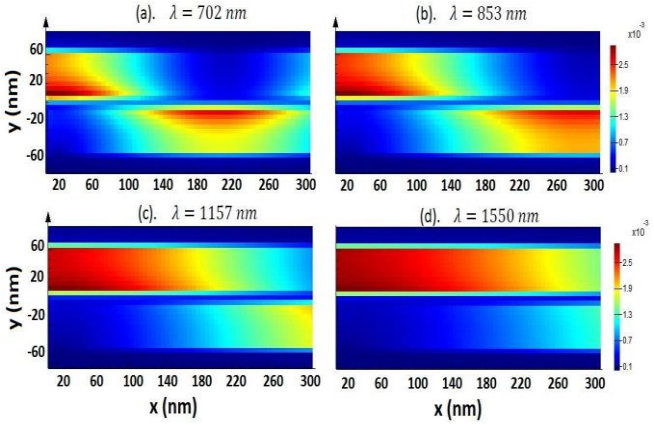

Fig. 4. Dynamics of contour profile of magnetic field in the plasmonic coupler. The field exchange between the waveguide-1 and waveguide-2 are shown by the colour map. Here, d = 9 nm and L = 300 nm (color online)

To reveal the effect of the separation between the waveguides on the transmittance spectra of the coupler we now fix the waveguide length L = 300 nm and change the separation between the waveguide as d = 6 nm, 9 nm, 12 nm, and 15 nm to record the transmittance spectra, which is shown in the Fig. 3. With the increase in waveguide separation '*d*' the power coupling or transfer of radiation between the waveguides becomes slower. In this case too the beam splitting point shifts towards higher wavelength (i.e. red-shift) for a longer coupler. As Fig. 2 suggests optimum wavelength and coupler length the current plots (Fig. 3) suggest suitable wavelength, separation between the waveguides and coupler length for beam splitting or complete power transfer purpose.

At this point portraying the electric and magnetic field profiles in the Plasmonic waveguide is in order. Both the fields extend into the metal and dielectric regions; however, remain confined within a depth less than their free-space wavelength. As per the boundary conditions, mentioned earlier, the longitudinal tangential component of the electric field E_x and transverse normal component of the magnetic field H_y are continuous across the interfaces, while the normal component of the electric field and parallel component of the magnetic field are discontinuous. Thus, it is useful to portray the magnetic field profile in the plasmonic waveguide coupler. The contour profile of the magnetic field in the coupler of waveguide-1 and waveguide-2 is shown in Fig. 4. For the simulation the width of waveguide separation '*d* ' is kept at 9 nm and the length of the waveguides '*L*' is fixed to 300 nm. We use the input EM radiation of wavelength as λ = 702 nm, 853 nm, 1157 nm and 1550 nm (bit arbitrarily spread over a wide range). The dynamics of the field shows quicker coupling at smaller wavelengths.

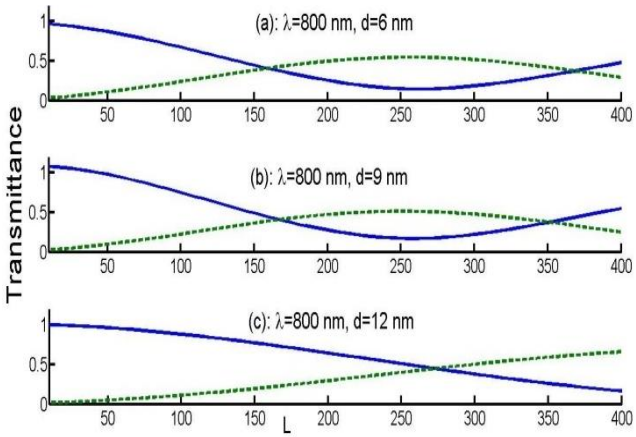

Fig. 5. Transmittance along waveguide/coupler length for λ=800 nm. (a) d = 6 nm, (b) d = 9 nm, and (c) d = 12 nm. Here the solid line is for waveguide-1 and the dotted line is for waveguide-2 (color online)

We now show the power exchange dynamics in the plasmonic waveguide coupler along the coupler length. The transmittances in the waveguides are plotted with respect to the coupler length in Fig. 5 for different separation of the waveguide, namely, d = 6 nm, 9 nm and 12 nm keeping the the wavelength of the EM radiation fixed to λ = 800 nm. An increasing separation ' *d* ' needs longer coupling length (the length of complete power exchange). However, in this plasmonic waveguide coupler complete power exchange is not visible.

To describe the role of operating wavelength on the power exchange dynamics we plot the transmittance with respect to the coupler length at different values of λ = 600 nm, 800 nm, 1200 nm and 1500 nm but with a fixed

waveguide separation d = 9 nm (Fig. 6). Two distinct features become obvious; firstly the coupling length is smaller for smaller wavelength and secondly, the amount of power exchanged is greater for larger wavelength. In fact, at lower wavelength the power exchange dynamics is asymmetrical in the waveguides. Thus, one needs to optimize the wavelength for the desired result and purpose.

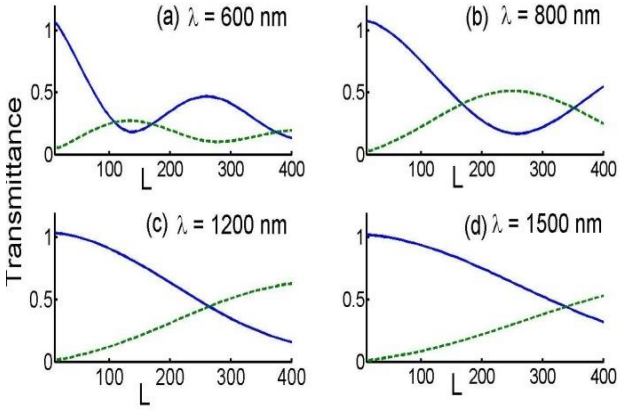

Fig. 6. Transmittance along waveguide/coupler length for d = 9 nm. (a) λ = 600 nm, (b) λ = 800 nm, (c) λ = 1200 nm, and (d) λ = 1500 nm. The solid and dotted lines are for waveguide-1 and waveguide-2 respectively (color online)

4. Conclusion

We investigated the transmission properties of a plasmonic waveguide coupler (created by a five-layer MIMIM) using FDTD simulation. The power transfer in such plasmonic coupler is very sensitive to the operating wavelength, which can be manipulated for sensing and even data processing purposes. The total length of the coupler as well as the separation of the plasmonic waveguides significantly control the power exchange dynamics, beam splitting phenomena and overall coupling. The results can be helpful to fabricate a miniature plasmonic waveguide coupler; furthermore, to optimize it in terms of the dimension and operating wavelength. Such miniature plasmonic coupler may be proven very useful for making plasmonic devices like filters, interconnects, all-optical switches, etc.

Acknowledgment

The author MM is thankful to DST-SERB for the research grant via fast track project no FTP/PS-211/2012. Soumendu Jana would like to acknowledge the financial supports of Ministry of Electronics and Information Technology, MeitY, Govt. of India, through "Young Faculty Research Fellowship under Visvesvaraya PhD Scheme" (Ref: MLA / MUM /GA / 10(37) B) and Science and Engineering Research Board (SERB), Govt. of India, through core research grant (File Number: CRG/2019/005073).

References

[1] S. A. Maier, "Plasmonics: Fundamentals and Applications", Springer, 2007.
[2] S. Zhu, G. Q. Lo, D. L. Kwong, Optics Express **20**, 15232 (2012).
[3] E. N. Economu, Phys. Rev. **182**, 539 (1969).
[4] R. H. Ritchie, Physical Review **106**(5), 874 (1957).
[5] M. A. Noginov, V. A. Podolskiy, G. Zhu, M. Mayy, M. Bahoura, J. A. Adegoke, B. A. Ritzo, K. Reynolds, Optics Express **16**(2), 1385 (2008).
[6] A. Polman, H. A. Atwater, Materials Today **8**, 56 (2005).
[7] J. N. Anker, W. P. Hall, O. Lyanders, N. C. Shan, J. Zhao, R. P. Van Duyne, Nature Mater. **7**, 442 (2008).
[8] N. Fang, H. Lee, C. Sun, X. Zhang, Science **308**, 534 (2005).
[9] E. Ozbay, Science **311**, 189 (2006).
[10] A. Hosseini, Y. Massoud, Opt. Express **14**(23), 11318 (2006).
[11] G. Veronis, S. Fan, Appl. Phys. Lett. **87**, 131102 (2005).
[12] H. Zhao, X. G. Huang, J. Huang, Phys. E **40**, 3025 (2008).
[13] S. Jana, S. Konar, M. Mishra, Zeitschrift fur Naturforschung - Section A Journal of Physical Sciences **63**, 145 (2008).
[14] D. Chelladurai, M. Doderer, U. Koch, Y. Fedoryshyn, C. Haffner, J. Leuthold, Opt. Express **27**, 11862 (2019).
[15] M. Olyaee, M. Tavakoli, A. Mokhtari, Opt. Quant. Electron **50**, 404 (2018).
[16] F. Ding, S. I. Bozhevolnyi, IEEE Journal of Selected Topics in Quantum Electronics **25**, 1 (2019).
[17] C. E. Garcia-Ortiz, V. Coello, E. Pisano, Y. Chen, S. I. Bozhevolnyi, Opt. Express **27**, 22753 (2019).
[18] S. Tan, A. Argondizzo, J. Ren et al., Nature Photon **11**, 806 (2017).
[19] A. Dolatabady, N. Granpayeh, Plasmonics **12**, 597 (2017).
[20] K. Leosson, T. Nikolajsen, A. Boltasseva, S. I. Bozhevolnyi, Optics Express **14**(1), 314 (2006).
[21] J. Tao, X.G. Huang, X. S. Lin, Q. Zhang, X. P. Jin, Opt. Express **17**(16), 13989 (2009).
[22] S. Bozhevolnyi, V. Volkov, E. Devaus, J. Laluet, T. Ebbesen, Nature **440**, 508 (2006).
[23] M. Futamata, Applied Optics **36**, 364 (1997).
[24] I. I. Smolyaninov, C. C. Davis, A. V. Zayats, New Journal of Physics **7**, 175 (2005).
[25] B. Sepulveda, L. M. Lechuga, G. Armelles, Journal of Lightwave Technology **24**, 945 (2006).
[26] J. J. Ju, S. Park, M. S. Kim, J. T. Kim, S. K. Park, Y. J. Park, M. H. Lee, Journal of Lightwave Technology **26**, 1510-8 (2008).
[27] P. Berini, I. De Leon, Nature Photonics **6**, 16 (2012).
[28] A. V. Zayats, I. I. Smolyaninov, A. A. Maradudin, Physics Reports **408**, 131 (2005).
[29] J. Zhang, L. Zhang, W. Xu, Journal of Physics D: Applied Physics **45**, 113001 (2012).
[30] Wei-Ping Huang, J. Opt. Soc. Am. A **11**, 963 (1994).
[31] Jin Tao, Xu Guang Huang, Xianshi Lin, Qin Zhang, Xiaopin Jin, Opt. Express **17**, 13989 (2009).

*Corresponding author: soumendu.jana@thapar.edu